PHYSICAL REVIEW B **87**, 140302(R) (2013)

Minimum thermal conductivity in superlattices: A first-principles formalism

Jivtesh Garg and Gang Chen
Department of Mechanical Engineering Massachusetts Institute of Technology, Cambridge, Massachusetts 02139, USA
(Received 12 February 2013; published 26 April 2013)

The thermal conductivity of silicon-germanium superlattices is computed from density-functional perturbation theory using relaxation times that include both anharmonic and interface roughness effects. A decrease in the group velocity of low-frequency phonons in addition to the interface-disorder-induced scattering of high-frequency phonons drives the superlattice thermal conductivity to below the alloy limit. At short periods, interplay between decrease in group velocity and increase in phonon lifetimes with increase in superlattice period leads to a minimum in the cross-plane thermal conductivity. Increasing the mass mismatch between the constituent materials in the superlattice further lowers the thermal conductivity below the alloy limit, pointing to avenues for higher efficiency thermoelectric materials.

DOI: 10.1103/PhysRevB.87.140302 PACS number(s): 66.70.−f, 63.20.dk, 63.20.kg, 63.22.Np

Superlattices have been experimentally measured to have low thermal conductivities, in some cases even lower than their homogeneous alloys.[1–3] The reduced thermal conductivity can lead to improvement in thermoelectric figure of merit[4] or impede the thermal management of semiconductor lasers.[5] Mechanisms behind the thermal conductivity reduction have been studied using different models including Boltzmann transport equation,[6,7] lattice dynamics,[8–10] molecular dynamics,[11–13] and acoustic wave equation.[14] These models, however, lack predictive power and are usually based on a specific sets of assumptions. For example, Boltzmann equation based models neglect phonon coherence and its consequences on phonon band structure modification, while lattice dynamics and acoustic wave approaches usually neglect the effect of interfacial disorder on phonon scattering. Molecular dynamics simulation is based on classical potentials, which lack accuracy for thermal conductivity prediction.[15] Despite the drawbacks of these approaches, past modeling together with experimental studies have led to the general acceptance that interface roughness plays a strong role in the thermal conductivity reduction, while a reduction in group velocity maybe is important in the short-period limit.

Recently, a first-principles-based approach that relies upon the use of harmonic and anharmonic force constants derived from density-functional perturbation theory (DFPT)[16–18] has been developed for studying thermal conductivity in perfect crystals[19,20] as well as alloys.[21] Garg *et al.*[22] used this approach to compute the thermal conductivity of ideal Si/Ge superlattices with perfect interfaces from first principles and showed that the computed thermal conductivity first decreased and then reached a constant value with an increase in the superlattice period. Such a trend is consistent with previous lattice dynamics calculations[8,10] based on the use of empirical potentials. This behavior, however, is not consistent with experimental results[1] where the thermal conductivity is observed to increase with period at longer periods; this suggests the need to incorporate the effect of interfacial disorder in the prediction of superlattice thermal conductivity.

In this Rapid Communication, we combine the three effects—group velocity reduction, interfacial disorder, and intrinsic anharmonic phonon scattering—in a first-principles formalism to compute the thermal conductivity of Si/Ge superlattices with a growth direction along [001] and with a period of $2n$ atomic layers (n monolayers of Si $\times$ n monolayers of Ge) and explain a minimum in superlattice thermal conductivity at short periods. The interface effect is included in two ways. First, a large unit cell, spanning one period of the superlattice, includes phonon reflection and coherent wave superposition, leading to new phonon band structures. Second, interface roughness is simulated as a random mixing of Si and Ge atoms in a narrow region around the interface. This mass mixing is the dominant interfacial scattering mechanism for phonons at short periods.[23] To compute the interfacial scattering rates, we replace the disordered crystal with an ordered one and treat the disorder as a perturbation[24] (an idea proposed by Abeles[25] for alloys); the use of perturbation theory to compute scattering rates due to mass disorder has been found to yield excellent agreement with experiments.[21,26] The masses of the atoms in the relevant superlattice unit cell at the sites of disorder are taken to be the average of Si and Ge masses, the other atoms are assigned the mass of Si and Ge on either side of the interface respectively. We take the thickness of the disordered region to be four atomic layers based on Refs. 27 and 28. The second- and third-order interatomic force constants obtained from DFPT using the virtual crystal approximation,[29,30] where the atomic potential at each site is an average of Si and Ge potentials (the use of this approximation is validated in Ref. 22). The phonon modes of this unit cell are used to compute the frequencies, group velocities, populations, and lifetimes that enter into the calculation of thermal conductivity. Finally, we adopt the single-mode relaxation time (SMRT) approximation[31] as an approximate solution of the Boltzmann transport equation;[32] the thermal conductivity k_α (along direction α) is then given by

$$k_\alpha = \frac{\hbar^2}{N\Omega k_B T^2} \sum_\lambda c_{\alpha\lambda}^2 \omega_\lambda^2 n_\lambda (n_\lambda + 1)\tau_\lambda,$$

where c, ω, $\bar{n}$, and τ are the phonon group velocities, frequencies, equilibrium populations, and relaxation times, λ represents the vibrational mode $(\boldsymbol{q}j)$ ($\boldsymbol{q}$ is the wave vector and j the phonon branch), and T,$\boldsymbol{\Omega}$, and N are the temperature, cell volume, and size of the $\boldsymbol{q}$-point mesh used. The scattering rate, $1/\tau_\lambda$, of a phonon mode λ is taken to be the sum of a term describing scattering due to interfacial disorder $(1/\tau_{\lambda a})$

and a term describing anharmonic scattering $(1/\tau_{\lambda b})$ as in Matthiessen's rule.

The scattering rates due to interfacial disorder are calculated using perturbation theory:[20]

$$\frac{1}{\tau_{\lambda a}} = \frac{\pi}{2N}\omega_\lambda^2 \sum_{\lambda'} \delta(\omega_\lambda - \omega_{\lambda'}) \sum_\sigma g(\sigma)|\vec{e}(\sigma|\lambda')\vec{e}(\sigma|\lambda)|^2,$$

where σ denotes the atomic sites in the superlattice unit cell, g takes into account the magnitude of mass disorder and is defined as $g(\sigma) = \sum_i f_i(\sigma)[1 - m_i(\sigma)/\bar{m}(\sigma)]^2$, where i, f, and m are the atomic species, concentration, and mass respectively. $\bar{m}(\sigma)$ is the average mass at site σ and e represents the vibration eigenvector. $g(\sigma)$ is nonzero only for atomic sites in the region of disorder; the above equation therefore allows to compute the phonon scattering due to sublattice disorder, which is the case for interfacial disorder. Such a perturbative approach assumes point defect scattering in the region of interface and leads to an ω^4 dependence of scattering rates at low frequencies. Perfect reflection of phonons is accounted for by using the modified dispersion of the superlattice.

The anharmonic scattering rates are computed using the lowest-order three-phonon scattering processes in the SMRT approximation via[33]

$$\begin{aligned}\frac{1}{\tau_{\lambda b}} = \pi \sum_{\boldsymbol{q}'j'j} |V_3(-\boldsymbol{q}\,j,\boldsymbol{q}'\,j',\boldsymbol{q}''\,j'')|^2 \\ \times \{2(n_{\boldsymbol{q}'j'} - n_{\boldsymbol{q}''j''})\delta[\omega(\boldsymbol{q}\,j) + \omega(\boldsymbol{q}'\,j') - \omega(\boldsymbol{q}''\,j'')] \\ + (1 + n_{\boldsymbol{q}'j'} + n_{\boldsymbol{q}''j''})\delta[\omega(\boldsymbol{q}\,j) - \omega(\boldsymbol{q}'\,j') - \omega(\boldsymbol{q}''\,j'')]\},\end{aligned}$$

where $V_3(-\boldsymbol{q}\,j,\boldsymbol{q}'\,j',\boldsymbol{q}''\,j'')$ are the three-phonon coupling matrix elements.[33]

The harmonic and anharmonic force constants are obtained on a $10 \times 10 \times 10$ and $3 \times 3 \times 3$ supercells, respectively. For all density-functional perturbation theory calculations, an $8 \times 8 \times 8$ Monkhorst-Pack[34] mesh is used to sample electronic states in the Brillouin zone and an energy cutoff of 20 Ry is used for the plane-wave expansion. We carefully tested convergence of all measured quantities with respect to these parameters. First-principles calculations within density-functional theory are carried out using the PWscf and PHonon codes of the Quantum-ESPRESSO distribution[35] with norm-conserving pseudopotentials based on the approach of von Barth and Car.[36]

At the shortest period (11 Å) studied, both the cross-plane and in-plane thermal conductivity are computed to be 7 W/mK (see Fig. 1) at 300 K, significantly lower than the corresponding values for the superlattice with perfect interfaces,[22] 25 and 44 W/mK, respectively, at the same temperature (shown in the inset in Fig. 1). This indicates the dominant role played by interfacial disorder in reducing thermal conductivity in superlattices. Increasing the period decreases the cross-plane thermal conductivity to below 7 W/mK (see Fig. 1) and a minimum is observed at a period of 33 Å (in contrast with the prediction based on molecular dynamics simulations[12] where the cross-plane thermal conductivity of superlattices with rough interfaces was found to increase monotonically with period); along the in-plane direction, however, the thermal conductivity increases monotonically with period without exhibiting a minimum.

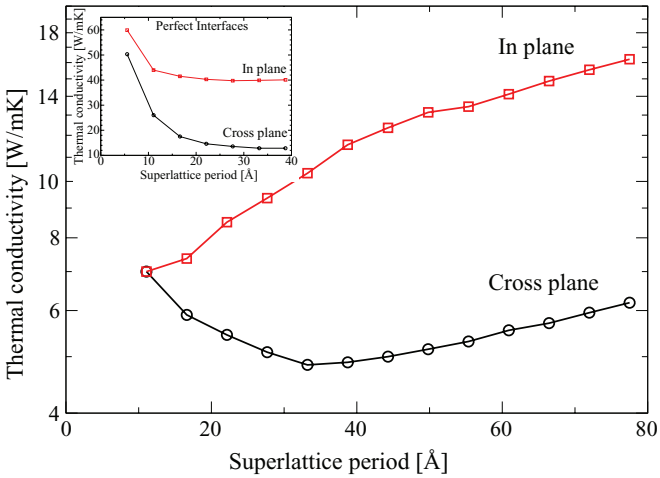

FIG. 1. (Color online) Computed in-plane and cross-plane thermal conductivity of Si/Ge superlattices as a function of superlattice period (Å) at 300 K. Inset shows the computed thermal conductivity of superlattices with perfect interfaces from Ref. 22 at the same temperature.

For the shortest period superlattice (11 Å), the computed thermal conductivity (7 W/mK at 300 K) is in excellent agreement with the measured value for $Si_{0.5}Ge_{0.5}$ alloy;[21] in this limit, interfacial disorder spans the entire superlattice making it essentially an isotropic alloy, the large reduction in thermal conductivity compared to pure Si and Ge is described in terms of the mass-disorder induced scattering of high-frequency phonons.[21] Increase in period beyond 11 Å thus results in the computed thermal conductivity to drop below the alloy limit (see Fig. 1). Experimentally, thermal conductivity of Si/Ge superlattices with periods between 30 and 275 Å was measured to be below that of the alloy film.[1] The thermal conductivity of superlattice with a period of 44 Å, computed here to be about 5 W/mK (see Fig. 1), is also in good agreement with the measured value of about 4 W/mK.[37] The small discrepancy can be attributed to the finite size of the experimental sample which leads to additional boundary scattering of phonons resulting in lower thermal conductivity, or the perturbative nature in our treatment of the atomic mixing at interface.

The formalism presented in this work allows an understanding of the above behavior through a microscopic characterization of the parameters involved in thermal transport. For this, we first compare the mean scattering rates of phonons due to anharmonicity and interfacial disorder for different superlattice periods in Fig. 2(a). Next, we look at

$$\gamma(\omega) \equiv \frac{1}{\Omega N} \sum_\lambda \delta(\omega - \omega_\lambda)\gamma_\lambda$$

to define the density of states weighted squared group velocity $\langle c^2 \rangle$, lifetimes $\langle \tau \rangle$, product of lifetimes and squared velocities $\langle c^2\tau \rangle$, and a spectral thermal conductivity $\tilde{k}(\omega) \equiv \langle c^2\omega^2\bar{n}(\bar{n}+1)\tau \rangle$, and compare different superlattices in terms of these parameters in Figs. 3 and 4.

Before describing the observed thermal conductivity behavior, we first point to another important consequence of this work, which relates to the significance of coherent phonons

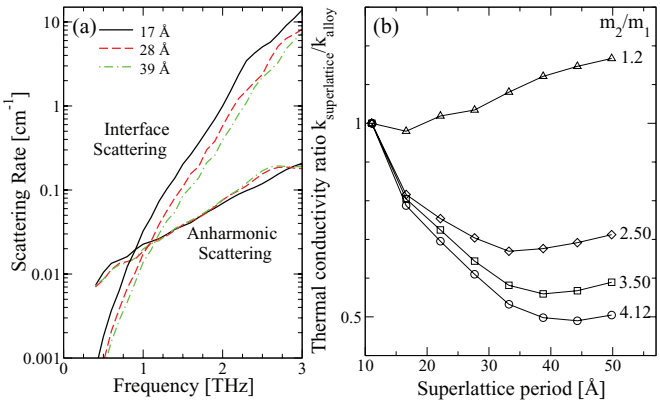

FIG. 2. (Color online) (a) Anharmonic and interfacial scattering rates at 300 K in superlattices of different periods (the numbers in the legend indicate superlattice period in Å). Interfacial scattering rates decrease with an increase in period resulting in an increase in phonon lifetimes with period (b) variation of cross-plane thermal conductivity at 300 K with mass mismatch between the constituent materials in the superlattice (mass ratio of 2.5 corresponds to Si/Ge superlattices).

in conducting heat. At low frequencies, phonons scatter mainly through the intrinsic three-phonon scattering processes, whereas at higher frequencies (beyond ∼1 THz), scattering due to interfacial disorder plays a more important role [see Fig. 2(a)]. At the cross-over between the two scattering processes (∼1 THz), the phonon mean-free path is estimated to be about 500 nm indicating that these phonons propagate much longer than the superlattice period and therefore undergo wave interference effects resulting in modified dispersion and hence coherent heat conduction.[38] We also find that in short period superlattices most of the heat is conducted by low-frequency phonons due to the strong interface scattering of high-frequency phonons. These low-frequency phonons have long mean free paths and conduct heat coherently. However, as the period is increased, higher frequency phonons begin to play a role pointing to a transition from coherent to incoherent transport.

We now address the computed thermal conductivity behavior. While interplay between phonon tunneling at short periods and decrease in interfacial scattering at longer periods was proposed as the mechanism for a minimum in cross-plane thermal conductivity by Yang *et al.*,[9] here we provide an accurate quantitative description of the phenomena and show the relative importance of the two effects at different periods and in different frequency regimes.

At short periods, increase in period reduces the ability of phonons to tunnel through the increasingly thicker layers of Si and Ge manifesting as a decrease in phonon group velocities [see Fig. 3(a)]. Simultaneously, the interface density decreases and leads to higher phonon lifetimes (due to reduced interface scattering) as shown in Fig. 2(a). The two have opposite effects on thermal conductivity. At short periods, the group velocity reduction dominates and leads to a decrease in thermal conductivity with increase in period. This can be seen more clearly in Figs. 3(a)–3(d) where it is evident that this decrease in thermal conductivity is driven by a decrease in the heat carrying ability of the low-frequency phonons [see Fig. 3(d)], while the higher-frequency phonons remain mostly unaffected.

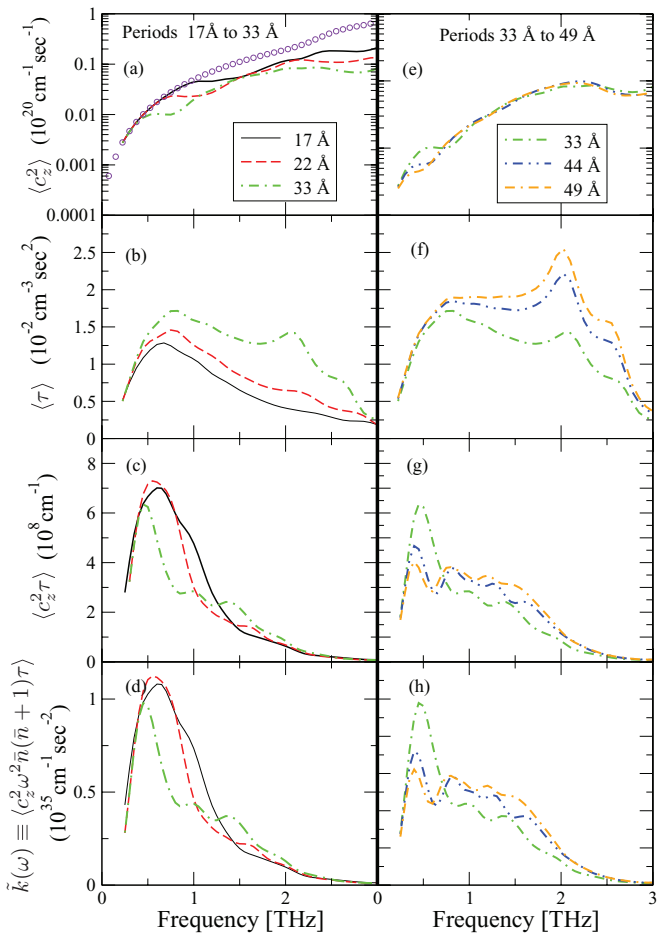

FIG. 3. (Color online) Density of states weighted: (a) and (e) squared cross-plane group velocity (open symbols are the group velocities in the bulk, which is an average of Si and Ge), (b) and (f) lifetimes, (c) and (g) product of squared velocity and lifetimes. (d) and (h) Effective cross-plane thermal conductivity $\tilde{k}(\omega)$.

This can be explained by noticing that at low frequencies the phonon lifetimes are determined by anharmonic scattering, which does not change significantly with period [see Figs. 2(a) and 3(b)]. Decrease in group velocities [see Fig. 3(a)] then drives the product $\langle c_z^2 \tau \rangle$ [see Fig. 3(c)] and, consequently, the thermal conductivity [see Fig. 3(d)] to lower values.

At longer periods [see Figs. 3(e)–3(h)], however, the net effect is an increase in thermal conductivity with increase

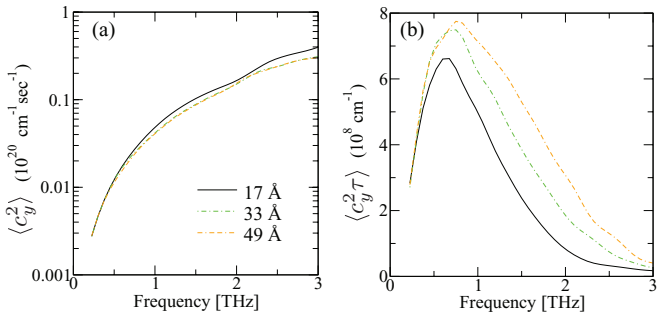

FIG. 4. (Color online) Density of states weighted: (a) squared in-plane group velocity and (b) product of squared velocity and lifetimes.

in period driven by an increase in the heat carrying ability of the higher frequency phonons. At these long periods, the effect of phonon tunneling saturates [see Fig. 3(e)] causing the group velocities to become relatively constant with respect to period [see Fig. 3(e)]. However, the decrease in interface density drives the phonon lifetimes to higher values [see Fig. 3(f)], which now cause the product $\langle c_z^2 \tau \rangle$ [see Fig. 3(g)] and, consequently, the thermal conductivity to increase with period [see Fig. 3(h)]. The opposite trends at short and long periods lead to a minimum in thermal conductivity at a period of about 30 Å (see Fig. 1).

Along the in-plane direction, the superlattice behaves more like a waveguide and the changes in phonon group velocity are minimal [see Fig. 4(a)]; decrease in interfacial scattering (increase in lifetimes) then results in a monotonic increase in the product $\langle c_y^2 \tau \rangle$ [see Fig. 4(b)] and, consequently, the thermal conductivity increases with period (see Fig. 1) without exhibiting a minimum.

While in alloys low thermal conductivity is achieved through disorder induced scattering that mainly reduces the heat carrying ability of the high frequency phonons,[21] here we have shown that in superlattices in addition to the presence of the above effect due to interfacial disorder [see Fig. 2(a)], the heat carrying ability of the low frequency phonons is reduced as well [see Fig. 3(d)] due to a decrease in their cross-plane group velocity [see Fig. 3(a)] causing the superlattice thermal conductivity to drop below the alloy value (see Fig. 1). The accuracy of the above formalism in predicting thermal conductivity in superlattices allows us to lay out design rules for low thermal conductivity materials. For example, while in the case of Si/Ge superlattices (mass ratio $m_2/m_1 = 2.5$), the minimum thermal conductivity is computed to be 30% below the alloy limit, increasing the mass ratio to 3.5 and 4.1 (while keeping the average mass the same as that in the Si/Ge superlattice) further lowers it to about 44% and 51% below the alloy value, respectively [see Fig. 2(b)], a result that holds key importance for high-efficiency thermoelectrics. On the other hand, as this ratio is decreased to about 1.2, this minimum almost disappears and the thermal conductivity increases monotonically with period [see Fig. 2(b)].

In conclusion, we have presented an approach to compute the thermal conductivity of superlattices in which all ingredients, vibrational modes and scattering rates, due to both anharmonicity and interfacial disorder are derived from first principles. By combining the effects of decrease in group velocity due to flattening of the phonon dispersion and increase in phonon relaxation times due to reduction in interfacial scattering as the period is increased we demonstrate a minimum in cross-plane thermal conductivity at short periods. At the shortest period studied, interfacial disorder extends across the entire superlattice and reduces the thermal conductivity to that of the alloy; increasing the period leads to a sharp decrease in group velocity along the cross-plane direction, which drives the cross-plane thermal conductivity to below the alloy limit; this followed by an increase in thermal conductivity at longer periods due to a decrease in interfacial phonon scattering results in a minimum being observed. Along the in-plane direction, however, the decrease in group velocity is modest and the increase in phonon lifetimes then results in a monotonic increase in in-plane thermal conductivity with period. Increasing the mass mismatch beyond that in the Si/Ge superlattice, shifts the minimum to longer periods and further lowers the thermal conductivity below the alloy limit—an effect that could have useful implications for high-efficiency thermoelectrics.

This material is based on work supported as part of the Solid State Solar-Thermal Energy Conversion Center (S3TEC), an Energy Frontier Research Center funded by the US Department of Energy, Office of Science, Office of Basic Energy Sciences under award DE-SC0001299/DE-FG02-09ER46577. J.G acknowledges and thanks Nicola Marzari and Nicola Bonini.

[1] S. M. Lee, D. G. Cahill, and R. Venkatasubramanian, Appl. Phys. Lett. **70**, 2957 (1997).
[2] G. Chen, C. L. Tien, X. Wu, and J. S. Smith, J. Heat Transfer **116**, 325 (1994).
[3] A. Majumdar, J. Heat Transfer **115**, 7 (1993).
[4] R. Venkatasubramanian, E. Siivola, T. Colpitts, and B. O Quinn, Nature (London) **43**, 597 (2001).
[5] M. A. Belkin, F. Capasso, A. Belyanin, D. L. Sivco, A. Y. Cho, D. C. Oakley, C. J. Vineis, and G. W. Turner, Nat. Photon. **1**, 288 (2007).
[6] G. Chen, Phys. Rev. B **57**, 14958 (1998).
[7] G. Chen, J. Heat Transfer **119**, 220 (1997).
[8] P. Hyldgaard and G. D. Mahan, Phys. Rev. B **56**, 10754 (1997).
[9] B. Yang and G. Chen, Phys. Rev. B **67**, 195311 (2003).
[10] S. I. Tamura, Y. Tanaka, and H. J. Maris Phys. Rev. B **60**, 2627 (1999).
[11] K. Imamura, Y. Tanaka, N. Nishiguchi, S. Tamura, and H. J. Maris, J. Phys.: Condens. Matter **15**, 8679 (2003).
[12] E. S. Landry and A. J. H. McGaughey, Phys. Rev. B **79**, 075316 (2009).
[13] S. Volz, J. B. Saulnier, G. Chen, and P. Beauchamp, Microelectron. J. **31**, 815 (2000).
[14] G. Chen, J. Heat Transfer **121**, 945 (1999).
[15] D. A. Broido, A. Ward, and N. Mingo, Phys. Rev. B **72**, 014308 (2005).
[16] A. Debernardi, S. Baroni, and E. Molinari, Phys. Rev. Lett. **75**, 1819 (1995).
[17] S. Baroni, P. Giannozzi, and A. Testa Phys. Rev. Lett. **58**, 1861 (1987).
[18] X. Gonze, Phys. Rev. A **52**, 1086 (1995).
[19] D. A. Broido, M. Malorny, G. Birner, N. Mingo, and D. A. Stewart, Appl. Phys. Lett. **91**, 231922 (2007).
[20] K. Esfarjani, G. Chen, and H. T. Stokes, Phys. Rev. B **84**, 085204 (2011).
[21] J. Garg, N. Bonini, B. Kozinsky, and N. Marzari, Phys. Rev. Lett. **106**, 045901 (2011).

[22]J. Garg, N. Bonini, and N. Marzari, Nano. Lett. **11**, 5135 (2011).
[23]S. P. Hepplestone and G. P. Srivastava, Phys. Rev. B **82**, 144303 (2010).
[24]S. I. Tamura, Phys. Rev. B **27**, 858 (1983).
[25]B. Abeles, Phys. Rev. **131**, 1906 (1963).
[26]W. A. Kamitakahara and B. N. Brockhouse, Phys. Rev. B **10**, 1200 (1974).
[27]R. L. Headrick and J.-M. Baribeau, J. Vac. Sci. Technol. B **11**, 1514 (1993).
[28]J.-M. Baribeau, J. Vac. Sci. Technol. B **16**, 1568 (1998).
[29]N. Marzari, S. de Gironcoli, and S. Baroni, Phys. Rev. Lett. **72**, 4001 (1994).
[30]S. Baroni, S. de Gironcoli, and P. Giannozzi, Phys. Rev. Lett. **65**, 84 (1990).
[31]J. M. Ziman, *Electrons and Phonons* (Oxford University Press, London, 1960).
[32]R Peierls, *Quantum Theory of Solids* (Clarendon Press, Oxford, 1955).
[33]G. Deinzer, G. Birner, and D. Strauch, Phys. Rev. B **67**, 144304 (2003).
[34]H. J. Monkhorst and J. D. Pack, Phys. Rev. B **13**, 5188 (1976).
[35]P. Giannozzi *et al.*, J. Phys.: Condens. Matter **21**, 395502 (2009); http://www.quantum-espresso.org.
[36]A. Dal Corso, S. Baroni, R. Resta, and S. de Gironcoli, Phys. Rev. B **47**, 3588 (1993).
[37]T. Borca-Tasciuc, W. L. Liu, J. L. Liu, T. Zeng, D. W. Song, C. D. Moore, G. Chen, K. L. Wang, M. S. Goorsky, T. Radetic, R. Gronsky, T. Koga, and M. S. Dresselhauss, Superlattices Microstruct. **28**, 199 (2000).
[38]M. N. Luckyanova, J. Garg, K. Esfarjani, A. Jandl, M. T. Bulsara, A. J. Schmidt, A. J. Minnich, S. Chen, Mildred. S. Dresselhaus, Z. Ren, E. A. Fitzgerald, and G. Chen, Science **338**, 936 (2012).